Secondary Circulation in the Faroe Bank Channel Outflow

GREGORY C. JOHNSON AND THOMAS B. SANFORD

Applied Physics Laboratory and School of Oceanography, College of Ocean and Fishery Sciences, University of Washington, Seattle, Washington

15 May 1991 and 2 October 1991

ABSTRACT

Data from a CTD station and three expendable current profiler drops at the center of the sill of the Faroe Bank Channel are used to examine the structure of the northwestward outflow of cold, relatively fresh, dense water from the Norwegian Sea into the Atlantic Ocean. A bottom boundary layer is present and exerts a bottom stress estimated at 3.5 Pa using observations in the log-layer. The shear at the interface between the outflow water and the water above is sufficiently strong to overcome the stratification and generate shear instabilities. The large stress at the bottom boundary creates an Ekman layer and thus a secondary cross-channel flow to the southwest there. A flow of similar magnitude but to the northeast is found in the high shear region at the interface. Hence, these data suggest a spiral velocity pattern in the outflow, created by the Ekman flow in the bottom boundary layer and cross-channel flow at the interface. This proposed circulation scheme explains the pinching of the density field observed at the southwest channel wall in CTD sections across the channel.

1. Introduction

Investigators in the 1960s discovered a northwestward outflow of cold, relatively fresh, dense water from the Norwegian Sea into the North Atlantic through the Faroe Bank Channel. An excellent review of early work is given by Borenäs and Lundberg (1988). Their analysis of a CTD (conductivity–temperature–depth) and "Pisa"-type current meter survey of the region resulted in an estimated 1.5×10^6 m^3 s^{-1} of outflow colder than 3°C during May 1983. Hydraulic control theory was applied to predict the transport of the outflow.

Analysis of data from combined CTD and ADCP (acoustic Doppler current profiler) surveys in spring 1987 and spring 1988 and a current meter array deployed during the intervening year resulted in an estimate of 1.9×10^6 m^3 s^{-1} for the outflow colder than 3°C (Saunders 1990). The current meter data indicated that the outflow was fairly steady. The velocities and temperatures measured by the array were used to calculate a time series of gradient Richardson numbers (Ri) over a 200-m interval. These estimates were low enough at times to suggest shear instabilities as a possible mixing mechanism at the interface between the inflowing and outflowing water. Water mass properties were shown to change significantly along the channel, arguably owing to this mixing.

Data from three expendable current profiler (XCP) drops and a CTD station in the center of the sill of the Faroe Bank Channel (Fig. 1) are used to describe previously undocumented features of the circulation in the channel. First we use these data to describe the bottom boundary layer (BBL) of the outflow and to estimate the bottom stress. Then we estimate values of Ri in the channel, which suggest that mixing owing to shear instabilities at the interface between the outflow and the warmer water above may be significant. Finally, we discuss the mean structure of the velocity and the density and how it is related to these secondary aspects of the circulation.

2. The data

Three XCPs (Sanford et al. 1982), numbers 738, 742, and 746, were dropped from the USNS *Kane* during cruise 270581 at the center of the sill of the Faroe Bank Channel (61.43°N, 8.34°W) at 4-hour intervals on 24 May 1981, just after CTD station 135161 had been occupied in the same location (Fig. 1). The probes reached the bottom at depths of 816 m, 828 m, and 821 m, respectively. The maximum CTD station pressure was 836 dbar. The temperature and velocity profiles for all three probes were similar, showing a cold outflow moving northwestward below a warm inflow moving southeastward, as expected.

A third-order polynomial is fit for density anomaly (σ_t) against temperature using the 1-dbar CTD station data. The relation is similar to that documented in recent investigations (Borenäs and Lundberg 1988; Saunders 1990). The standard deviation of the σ_t values from the fit and σ_t values from the CTD is 0.007 kg m^{-3}. This polynomial is applied to the temperature

Corresponding author address: Dr. Gregory C. Johnson, Applied Physics Laboratory, College of Ocean and Fishery Sciences, University of Washington, 1013 NE 40th St., Seattle, WA 98105.

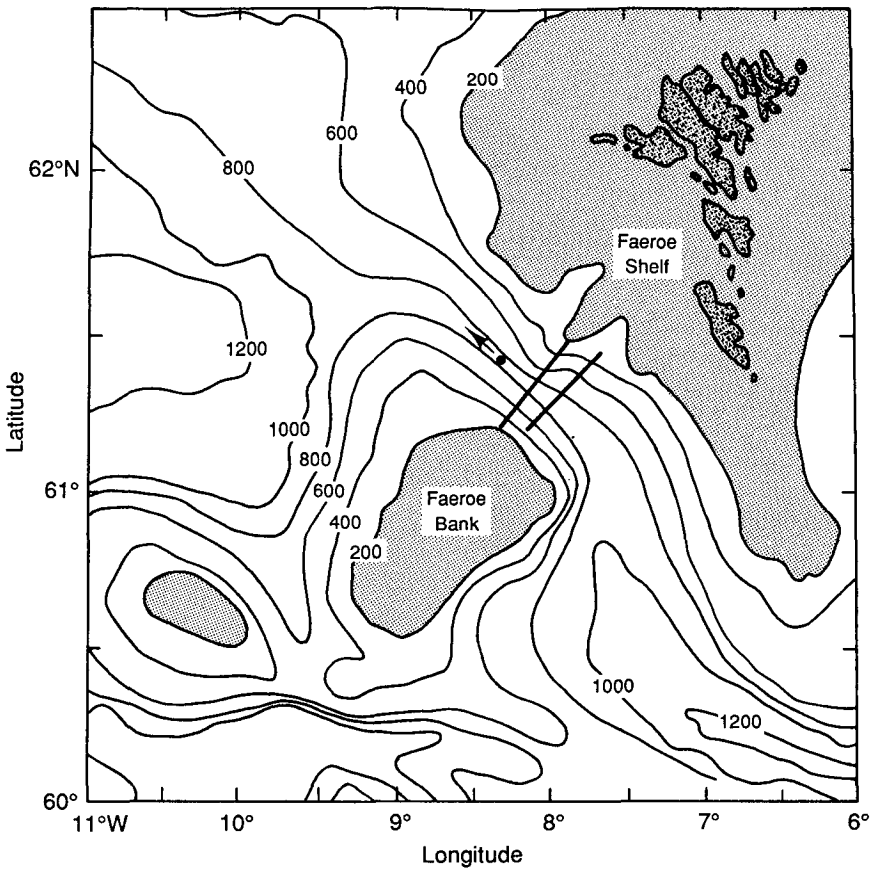

FIG. 1. The bathymetry of the Faroe Bank Channel at 200-m intervals (IHO/IOC/CHS 1984). The locations of the CTD station and XCP drops at the center of the channel sill (61.43°N, 8.34°W) are within the large dot. The arrow direction indicates the downstream coordinate axis 311°T, which is closely aligned with the isobaths. The straight line closest to the arrow gives the location of the section profiles in the bottom panel of Fig. 6, and the more distant line gives the location of the section profiles in the top panel of Fig. 6.

profiles (sorted to eliminate inversions) from the individual XCP drops to gain rough σ_t profiles for each drop.

The XCP profiles are processed such that a value of velocity, temperature, and σ_t is obtained for each probe rotation, one value roughly every 2/3 m. The barotropic velocity is not known, so for each drop the mean is removed, leaving the baroclinic velocity. To better exhibit the layered structure in the velocity, the coordinate system is rotated from magnetic north and east into downstream and cross-stream directions using the mean of the angle of the shear between 100–200-m and 650–750-m levels for the three drops. The resulting downstream direction is roughly northwestward at 311°T (±3°). The cross-stream direction is thus 41°T (northeastward). The downstream axis is indistinguishable from the topographically defined downchannel axis (Fig. 1).

Since the three drops show remarkably similar temperature and velocity structure, a set of mean profiles is constructed by first interpolating the data from the individual profiles onto an evenly spaced grid at 2/3-m intervals, starting at the bottom data point. The XCP records indicate that each probe hit the bottom before its wire broke. Hence, the XCP geometry dictates that the bottom data point of each probe is 1 m (±1/3 m) above the bottom. The evenly spaced depths, temperatures, density anomalies, and velocities for the three probes are averaged as a function of height above the bottom. This averaging scheme matches the profiles better than averaging on a temperature grid or on a depth grid; it also best preserves features in the BBL, since they depend on height above the bottom. The resulting profile is filtered with a 7-point Hanning filter (2-m half-width) to reduce noise for display.

The temperature profile (Fig. 2) shows a warm upper layer of roughly constant temperature (7.5°–8.5°C) over the top 400 m. From 400 to 760 m the temperature drops to −0.5°C, an 8°C change. The vertical temperature gradient is highest between 500 and 600 m. Between about 760 m and the bottom (822 m) the temperature is homogeneous. In this BBL σ_t is very

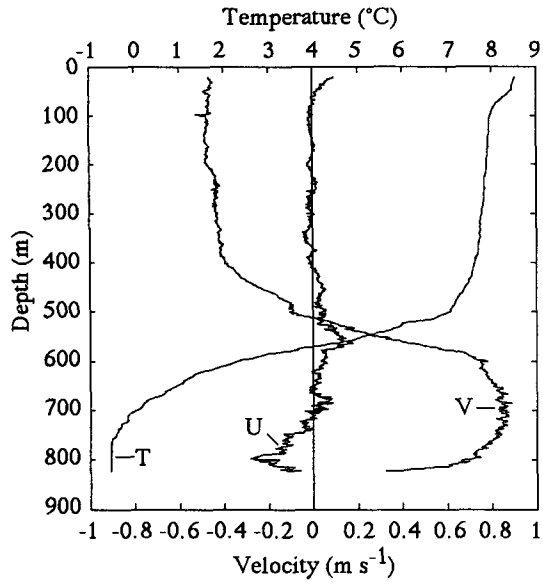

FIG. 2. The mean 2-m smoothed in situ temperature (T, °C), downstream velocity (V, m s^{-1}, 311°T), and cross-stream (U, m s^{-1}, 41°T) velocity profiles plotted against depth. The stratification of the interface between the warm upper layer and the colder outflow water is strongest between 500 and 600 m. Below about 760 m in the BBL, the temperature is homogeneous. The outflow water moves downstream and the water above upstream with a large vertical shear between them. Downstream velocity decreases below about 750 m in the BBL. Significant cross-stream velocities are observed at the depths of large downstream shear, at the interface, and in the BBL.

high, nearly 28.1 kg m^{-3}. The downstream velocity (Fig. 2) also exhibits a gross three-layer structure. It is roughly constant in the upper layer from the surface to 400 m and again in the lower layer between 650 and 750 m. The velocity increases about 1.2 m s^{-1} to the northwest between 400 and 650 m. Again, the highest vertical gradient is in the interfacial layer at 500–600 m. Below 750 m the velocity decreases rapidly toward the bottom in the BBL. The cross-stream velocity (Fig. 2) is much smaller in magnitude than the downstream velocity. It also has a different pattern. The regions of high cross-stream velocity are found where the downstream velocity has large shear. There is northeastward flow at the interfacial layer between the warm and cold layers (500–600 m) and a southwestward flow in the BBL (below 750 m).

3. Analysis

The BBL is examined and log-layer dynamics applied to estimate a bottom stress. Estimates of Ri are calculated over 10-m intervals using smoothed data from the individual drops, and the shear at the interface is found to be strong enough to allow generation of shear instabilities in spite of the stratification there. The effect of the stress at the BBL and the mixing at the interface on the mean circulation is discussed. The relation of this circulation to the details of the density structure seen in prior observations is also examined.

a. The bottom boundary layer

The unfiltered velocity profiles from each of the three drops are used in the BBL analysis. As in the mean profile (Fig. 2), the temperature is homogeneous up to 50–70 m above the bottom and the velocity increases rapidly away from the bottom. There is an anticyclonic veering with depth over the bottom 120 m, which is indicative of an Ekman spiral (Figs. 2 and 3). The observed spiral looks like the theoretical prediction for a mixed planetary boundary layer with log-layer and Ekman-layer dynamics [Holton 1979, Eq. (5.27)]. Using a surface wind direction of 22.5°, a BBL depth of 150 m, and a geostrophic velocity of 0.8 m s^{-1} in this equation gives a good match between the predicted and observed velocities.

The bottom 30 m of each drop, where the shear is unidirectional at 23° ± 4° west of the downstream direction, is amenable to log-layer analysis. This angle is close to the expected direction of 22.5°. Assuming the velocity in the bottom 30 m is of the form

$$u = \frac{u_*}{\kappa} \ln\left(\frac{z}{z_0}\right)$$

allows a least-squares linear fit of the velocity to the natural logarithm of the height above the bottom for each of the drops (Fig. 4). Here u is the velocity, u_* is the frictional velocity, $\kappa = 0.4$ is the von Kármán con-

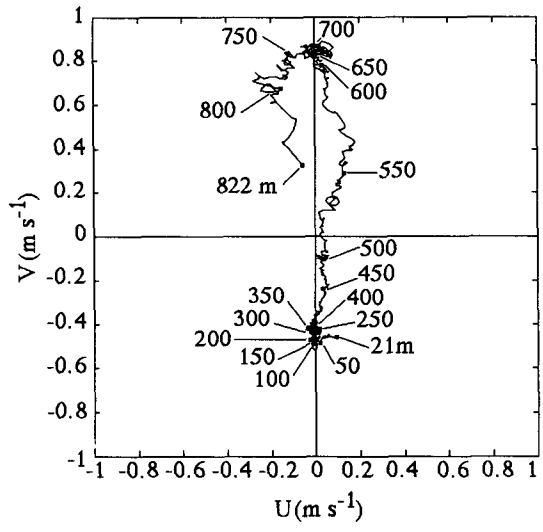

FIG. 3. Hodograph of the mean velocity smoothed over 2 m. The outflow core is between 650 and 750 m, and the roughly uniform inflow is between 21 and 400 m. Below the outflow core, the velocity spirals toward the bottom (822 m) in an Ekman-like fashion, with cross-stream flow to the southwest. In the high-shear region between the outflow and the inflow (500–600 m), the velocity curve indicates northeast cross-stream flow.

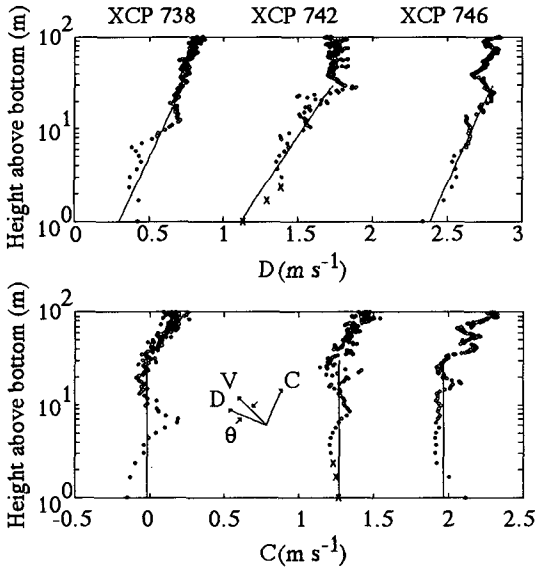

FIG. 4. Velocity plotted against the log of height above the bottom. The data from XCP 738 are plotted at the origin, those from 742 are offset 1 m s^{-1}, and those from 746 are offset 2 m s^{-1}. The velocities are rotated by 23° ± 4° to the west of the downstream direction (Fig. 1), as shown in the schematic in the bottom panel. This rotation is such that the component shown in the top panel contains all the shear in the bottom 30 m (D, m s^{-1}) and that in the bottom panel contains none in that depth range (C, m s^{-1}). The solid lines are the linear least-squares fits of the unfiltered velocities against the natural log of height above the bottom over the bottom 30 m. The more the lines in the top panel deviate from the vertical, the larger the estimates of the frictional velocity (0.057 ± 0.010 m s^{-1}) and bottom stress (3.5 ± 1.3 Pa). The velocities displayed from XCP 742 are smoothed over 2 m, since that drop was noisy. The x's indicate where the filter encountered padding of the record with the bottom value of velocity to allow the filtering of that bottom value.

stant, z is the height above the bottom, and z_0 is a roughness length [Holton 1979, Eq. (5.16)]. The frictional velocity u_* can be estimated for each drop by using the equation above. This procedure has been examined in other XCP profiles by Jones (1989). Since the barotropic velocity is not known, z_0 is not estimated. The frictional velocity estimated from the mean of the unsmoothed profiles is $u_* = 0.057 \pm 0.010$ m s^{-1}, which translates into a bottom stress of $\tau_x = \rho u_*^2 = 3.5 \pm 1.3$ Pa, where $\rho = 1027$ kg m^{-3} is the mean density. Averaging the profiles before performing the log-layer analysis gives similar results.

The linear spindown time for the outflow indicated by this analysis is $t_{spin} = Hu/2u_*^2$ [Gill 1982, from Eq. (9.12.7)]. If we take an outflow layer depth $H = 250$ m, an outflow velocity $u = 0.85$ m s^{-1}, and a frictional velocity $u_* = 0.057$ m s^{-1}, the spindown time is about 9 h. From Ekman theory the spindown time is about $t_{spin} = \pi H/4fh_{umax}$ [Holton 1979, from Eq. (5.35)]. Here the Coriolis parameter is $f = 1.3 \times 10^{-4}$ s^{-1} and the height above the bottom where the cross-stream velocity is a maximum is $h_{umax} = 25$ m, so the spindown time is about 17 h. Both of these times are very short and indicate that a large bottom drag is acting on the outflow.

The BBL in the channel, extending over about 120 m, is remarkably thick in comparison with previous observations of 10-m thickness on the Florida Shelf (Weatherly and Martin 1978). Some difference in thickness is to be expected, since the velocity in the outflow is about four times that on the Florida Shelf and the buoyancy frequency in the outflow is about one-fifth of that there. In fact, applying the values of $u_* = 0.057$ m s^{-1}, $f = 1.3 \times 10^{-4}$ s^{-1}, and $N^2 = 8.0 \pm 3.4 \times 10^{-6}$ s^{-2} (the average of the 10-m values described directly below from 650–700-m depth, just above the BBL in the interior) to the equation predicting the thickness of the BBL, $h = u_*/f[1 + N^2/f^2]^{1/4}$ [Weatherly and Martin 1978, Eq. (17′)] gives $h = 120 \pm 20$ m for a BBL thickness. This prediction is in good agreement with the observed thickness, perhaps somewhat fortuitously since the values of N^2/f^2 here are 2.5 ± 1 times the maximum values used to obtain the formula. Nonetheless, the thickness is plausible given the extreme conditions in the channel.

b. *The interface*

At the interface between the upper and lower layer the large velocity gradient suggests that shear instabilities may be mixing the two water masses. To investigate this possibility, we compute estimates of Ri from the individual drop profiles. Here the gradient Richardson number is the buoyancy frequency over the shear squared, or

$$\mathrm{Ri} = \frac{-\frac{g}{\rho}\frac{\partial \sigma_t}{\partial z}}{\left(\frac{\partial u}{\partial z}\right)^2 + \left(\frac{\partial v}{\partial z}\right)^2},$$

where $g = 9.8$ m s^{-2} is the gravitational constant.

Small-scale temperature inversions are present in the individual profiles, either owing to overturnings resulting from shear instabilities or compensating salinity variations not included in the temperature–density anomaly relation used to generate σ_t profiles for the probes. These features tend to reduce the buoyancy frequency. Small-scale velocity fluctuations will tend to make the shear squared larger. Both of these effects may bias the Ri estimates toward smaller values owing to noise. To minimize these effects and still maintain high vertical resolution, the individual XCP temperature profiles are sorted to remove inversions before generating σ_t profiles, and then the σ_t and velocity profiles are smoothed with a 31-point Hanning filter (10-m half-width) and subsampled at 10-m intervals. The terms of Ri are estimated using first differences of these subsampled profiles.

The results are displayed as a log–log scatterplot of the square of the vertical shear against the square of

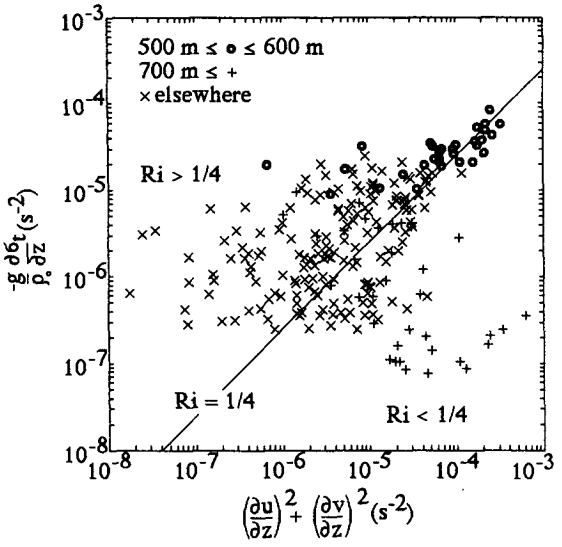

FIG. 5. Log–log scatterplot of 10-m first-difference square of the shear against buoyancy frequency squared. The solid line indicates a gradient Richardson number of Ri = 1/4. Points to the lower right of this line have smaller values and are unstable to shear instabilities. Points to the upper left of the line have larger values and are more stable. The o's are estimates in the high-shear high-stratification region in the interface between the layers (500–600 m). These estimates cluster around the line, indicating that shears in this region are large enough to allow shear instabilities to form in spite of the stratification. The +'s are estimates in the BBL (below 700 m), and the x's are estimates in the remainder of the water column.

the buoyancy frequency (Fig. 5). The solid line indicates Ri = 1/4, with points to the lower right being smaller (susceptible to shear instabilities) and to the upper left being larger (stable). The o's, most of which fall about Ri = 1/4, are estimates in the high-shear high-stratification interface region of 500–600-m depth (75% fall in the interval $1/8 < \text{Ri} < 1/2$). This tendency indicates that the shear in the interface is strong enough to allow the formation of shear instabilities, despite the stratification. Estimates where $\text{Ri} \ll 1/4$ are mostly in the BBL (the +'s, below 700 m), where the stratification is weak and the shear strong (over 73% have $\text{Ri} < 1/4$). Being in the BBL, these low values of Ri do not suggest mixing by interfacial shear instabilities. The ×'s, in the remaining part of the water column, are mostly stable to shear instabilities indicating little mixing outside the interface and BBL (over 78% have $\text{Ri} > 1/4$).

A *T–S* diagram of the CTD data reveals an intermediate water mass in the interface between the warm inflow water and the cold outflow water (similar to Borenäs and Lundberg 1988, their Fig. 2). The intermediate water mass lies outside of the line between the warm and cold end members on the *T–S* diagram, so it is difficult to see how there could be strong mixing between the upper and lower layers at the interface. The answer lies in the evolution of the *T–S* curves along the channel axis (Sanders 1990, his Fig. 15). Upstream of the sill the intermediate water mass causes a strong deviation from linearity in the curve. At the sill this deviation is much reduced. Downstream of the sill the curve is fairly linear, indicating obliteration of the *T–S* properties of the intermediate water mass through mixing near the sill.

c. *The overall structure*

The XCP profiles clearly show the three-layer structure of the circulation in the channel. The cold, dense outflow water moves northwestward, with the warmer water above moving in the opposite direction and an interface with strong stratification and shear between (Fig. 2). The profiles also reveal a more detailed picture of the circulation.

A thick BBL is present, with a 30-m log-layer (Fig. 4), a 50–70-m region of homogeneous temperature (Fig. 2), and an Ekman-like veering of the velocity vector over 120 m (Figs. 2 and 3). The bottom stress exerted on the outflow is quite large. In the bottom 120 m it causes a southwestward cross-stream transport per unit width of about 1/16 the magnitude of the outflow transport. The peak cross-stream velocity is about 1/4 that of the downstream flow, and the depth range over which it occurs is also about 1/4 that of the outflow.

At the interface between the layers the shear is strong enough such that shear instabilities may effect significant mixing there. Again, the velocity veers in the high shear region, here between 500 and 600 m (Figs. 2 and 3). This pattern suggests that mixing is associated with a cross-stream velocity and transport per unit width similar to that in the BBL but in the opposite direction.

This secondary circulation with opposite flows at the top and bottom of the outflow suggests a spiral character in the outflow. That is, as the dense cold water flows out of the channel, it experiences a frictional force at the BBL, which causes a cross-stream flow. This water moves southwestward in the BBL and may upwell at the southwestern wall of the channel. If it then reaches the interface, it may travel northeastward along the interface in the high-shear region, undergoing considerable mixing and warming.

If we assume the barotropic velocity is not too far from zero, these cross-stream flows each carry about 1/16 as much fluid as the downstream outflow, with 1/4 the velocity over 1/4 the depth of the outflow. Assuming that this secondary circulation exists only in the vicinity of the sill, where the flow is strongly confined, the ratio of the width of the channel at 500-m depth where the probes were dropped (20 km) to the length over which the channel remains narrow (about 80 km) is about 1/4 (Fig. 1). This geometry indicates that a fluid parcel that stays in the boundary layers might move through one turn of the spiral as it travels down the channel in the outflow. About 1/4 of the net outflow takes part in this spiral. If this fraction is

warmed to about the mean of the inflow and outflow temperatures, as the profiles suggest, the outflow temperature is significantly modified by this secondary circulation. A significant warming of the outflow along the channel is seen in analyses of previous CTD surveys (Saunders 1990).

4. Conclusions

The suggested spiral pattern explains a puzzling detail of previous cross-channel temperature sections (Fig. 6). The isotherms, while tilted in the correct sense for the downstream outflow to be geostrophic, are often pinched at the southwest wall of the channel and spread toward the northeast wall (Borenäs and Lundberg 1988; Saunders 1990). If the cross-channel flow in the BBL were to upwell upon reaching the southwest channel wall, the upwelling would be large enough to create the sharp pinching of the isotherms observed. The northeastward cross-stream flow at the interface combined with the mixing there suggests that if this sharp gradient were advected away from the wall, mixing would spread the gradient to the northeast, as observed. The apparent importance of bottom friction and mixing in maintaining the temperature structure differs from the inviscid theory proposed to explain a similar feature in flow through the Vema Channel (Hogg 1983).

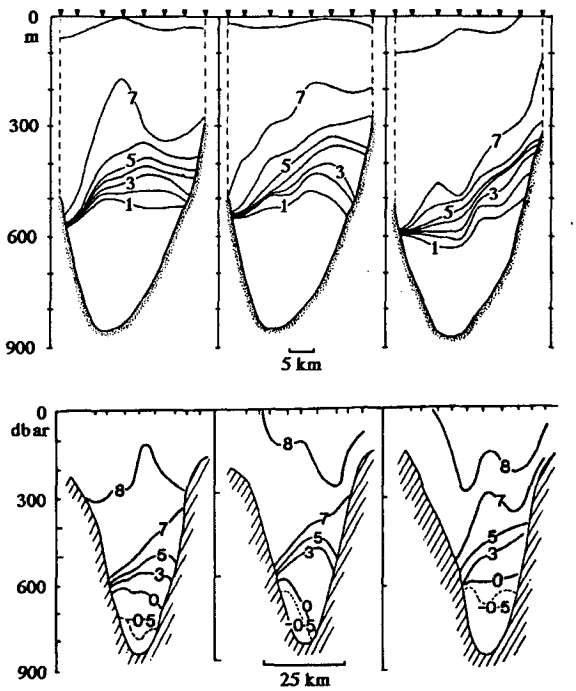

FIG. 6. Section profiles of potential temperature from a series of CTD sections made across the Faroe Bank Channel near the XCP drops. The southwest wall is to the left, where the pinching of the isotherms that may be present owing to upwelling of the southwestward flow in the BBL can be seen. The isotherms spread to the northeast, probably owing to mixing through shear instabilities there. The outflow velocity increases toward the bottom, as indicated by the sloping isotherms. The top set of profiles is adapted from Fig. 7 of Borenäs and Lundberg (1990), and the bottom set is adapted from Figs. 6, 7, and 8 of Saunders (1990). See Fig. 1 for section locations.

An argument against strong frictional influence at the ocean bottom is presented by MacCready and Rhines (1991), who show that in the presence of stratification and bottom slope, the cross-stream flow in the Ekman layer will eventually set up a density field that reduces velocity near the bottom geostrophically rather than frictionally. This effect is possible only where there is both bottom slope and stratification, and the isotherms do appear to reverse slope in the interface close to the northeast channel wall at times (Fig. 6). The interface is too sharp at the southwest channel wall to make any speculations about the applicability of the theory there. However, in the center of the channel, where the largest mass of cold water is found, there is little bottom slope and almost no stratification, so such an adjustment is not likely for the bulk of the outflow. Hence, it is improbable that this effect reduces the stress from the estimate obtained here.

Our data analysis suggests that a great deal of stress, about 3.5 ± 1.3 Pa, is exerted at the bottom of the outflow. If the outflow water moves at 0.85 m s^{-1}, it will take about 26 h to flow through the 80-km channel, roughly two spindown times. Thus, the stress would stop the outflow well before it exited the channel if the strong pressure gradient that drives the outflow were removed. This pressure gradient is provided by the density difference between the top 850 m of the Atlantic Ocean and the Norwegian Sea. Indeed, Saunders (1990) points out that the existing pressure gradient is probably too large for the inviscid hydraulic control theory used to predict the volume transport through the channel (Borenäs and Lundberg 1988). He suggests that the use of an unrealistically low height of the upstream interface limits the transport prediction to a reasonable value. Our bottom-stress estimate provides further support to the assertion that inviscid hydraulic control theory is probably not applicable to the outflow. Any adequate model of the outflow through the Faroe Bank Channel will need to incorporate the significant influences of friction and mixing presented here.

Acknowledgments. We are indebted to the ship's company and the scientific parties on board USNS *Kane* for their assistance in gathering the data, especially Patrick McKeown and James Carlson. We thank Alan Brandt at the Office of Naval Research and Robert Rushton at NAVOCEANO for making the CTD data available. We were supported under Grant N00014-90-J-1100 from the Office of Naval Research. The Naval Ocean Research and Development Activity (now NOARL) purchased the XCPs. The comments of two reviewers improved the manuscript.

REFERENCES

Borenäs, K. M., and P. A. Lundberg, 1988: On the deep-water flow through the Faroe Bank Channel. *J. Geophys. Res.*, **93,** 1281–1292.

——, and ——, 1990: Some questions arising from the application of hydraulic theory to the Faroe Bank Channel deep-water flow. *Pure Appl. Geophys.*, **133,** 573–585.

Gill, A. E., 1982: *Atmosphere-Ocean Dynamics.* Academic Press, 662 pp.

Hogg, N. G., 1983: Hydraulic control and flow separation in a multilayered fluid with applications to the Vema Channel. *J. Phys. Oceanogr.*, **13,** 695–708.

Holton, J. R., 1979: *An Introduction to Dynamic Meteorology,* 2nd ed., Academic Press, 391 pp.

IHO/IOC/CHS, 1984: *General Bathymetric Chart of the Oceans,* 5th ed., International Hydrographic Organization/Intergovernmental Oceanographic Commission/Canadian Hydrographic Service, 74 pp., sheet 5.04.

Jones, D. W., 1989: Velocity Profiler (XCP) observations of a bottom boundary layer in the Strait of Juan de Fuca. Applied Physics Laboratory, University of Washington, Tech. Rep. APL-UW TR 8927, 209 pp.

MacCready, P., and P. B. Rhines, 1991: Slippery bottom boundary layers on a slope. *J. Phys. Oceanogr.,*

Sanford, T. B., R. G. Drever, J. H. Dunlap, and E. A. D'Asaro, 1982: Design, operation and performance of an Expendable Temperature and Velocity Profiler (XTVP). Applied Physics Laboratory, University of Washington, Tech. Rep. APL-UW TR 8110, 83 pp.

Saunders, P. M., 1990: Cold outflow from the Faroe Bank Channel. *J. Phys. Oceanogr.*, **20,** 29–43.

Weatherly, G. L., and P. J. Martin, 1978: On the structure and dynamics of the oceanic bottom boundary layer. *J. Phys. Oceanogr.*, **8,** 557–570.